Highly Efficient Electrogenerated Chemiluminescence of Au_{38} Nanoclusters

Mahdi Hesari, Mark Steven Workentin,* and Zhifeng Ding*

Department of Chemistry and Centre for Advanced Materials and Biomaterials Research, The University of Western Ontario, London, Ontario N6A 5B7, Canada

ABSTRACT An investigation of mechanisms for the near-infrared (NIR) electrogenerated chemiluminescence/electrochemiluminescence (ECL) of $Au_{38}(SC_2H_4Ph)_{24}$ (Au_{38}, SC_2H_4Ph = 2-phenylethanethiol) nanoclusters both in annihilation and coreactant paths is reported. Essentially, no ECL emission was produced in the annihilation route over the potential range of the accessible redox states of Au_{38}, because of the short lifetime and/or low reactivity of the electrogenerated Au_{38} intermediates necessary for ECL. Highly efficient light emission with a nominal peak wavelength of 930 nm in the NIR region was observed in the anodic region upon addition of tri-*n*-propylamine (TPrA) as the coreactant. The ECL mechanisms were elucidated by means of ECL—potential curves and spooling ECL spectroscopy. It was discovered that the Au_{38}^{+*} (and also Au_{38}^{3+*}) were electrogenerated as the major excited species in the light emission processes. Benzoyl peroxide was also used as a coreactant in the cathodic potential range from which benzoate radicals, with a high oxidizing power, were formed. These radicals accepted electrons from the electrogenerated Au_{38}^{2-} HOMO, resulting in the Au_{38}^{-*} excited state that emitted light at 930 nm. The photoluminescence of the various Au_{38} charge states, namely, Au_{38}^{2-}, Au_{38}^{-}, Au_{38}^{0}, Au_{38}^{+}, Au_{38}^{2+}, and Au_{38}^{4+}, electrogenerated *in situ*, indicated no significant difference in the emission peak wavelength. This information allowed a careful mapping of the relevant ECL mechanisms. It was found that the ECL efficiency could reach an efficiency of 3.5 times as high as that of the $Ru(bpy)_3^{2+}$/TPrA system.

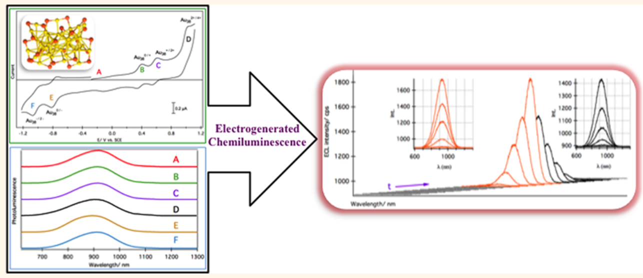

KEYWORDS: Au_{38} nanoclusters · NIR electrochemiluminescence · radical cations and anions · coreactant systems · spooling spectroscopy · photoluminescence

The distinct molecular-like properties of thiol-protected gold nanoclusters with a general formula $Au_n(SR)_m$ (n < 100, SR represents a thiol ligand) and their corresponding extraordinary optical,[1−6] electrochemical,[7−9] and catalytic[10−13] properties have made them the focus of a wide range of fundamental and practical studies.[6,14] Included among these studies are extensive efforts to synthesize and characterize novel Au core sizes and adjust the functionality of the protecting ligands, as a means to probe the various factors that alter the cluster properties.[15−18] Knowledge of the discrete optical and electrochemical characteristics permits investigations that explore the mechanisms of electrogenerated chemiluminescence or electrochemiluminescence (ECL) of these Au nanoclusters. ECL is a photoelectrochemical process, in which electrogenerated reactive species, radical cations or anions or other charged redox states of Au nanoclusters specifically here, participate in an electron transfer (ET) to produce excited states, which emit light upon relaxing to ground states.[19,20] The ECL light emission wavelength depends on the energy gap between the highest occupied molecular orbital (HOMO) and lowest unoccupied molecular orbital (LUMO). ECL signals, which do not require a laser light source,[21] have been used for a wide range of electroanalytical detections mainly due to their high signal-to-noise ratio.[22,23] The ECL emission can be generated and controlled *via* a working electrode potential, in order to trigger a specific detection in a mixture of analytes.[24]

We have recently reported the ECL observed from $Au_{25}(SR)_{18}^{+}$ in both annihilation and coreactant routes.[25] These ECL peak wavelengths were found to be in the near-infrared (NIR) region, which correlated

* Address correspondence to zfding@uwo.ca, mworkent@uwo.ca.

Received for review June 11, 2014 and accepted August 3, 2014.

Published online August 03, 2014
10.1021/nn503176g

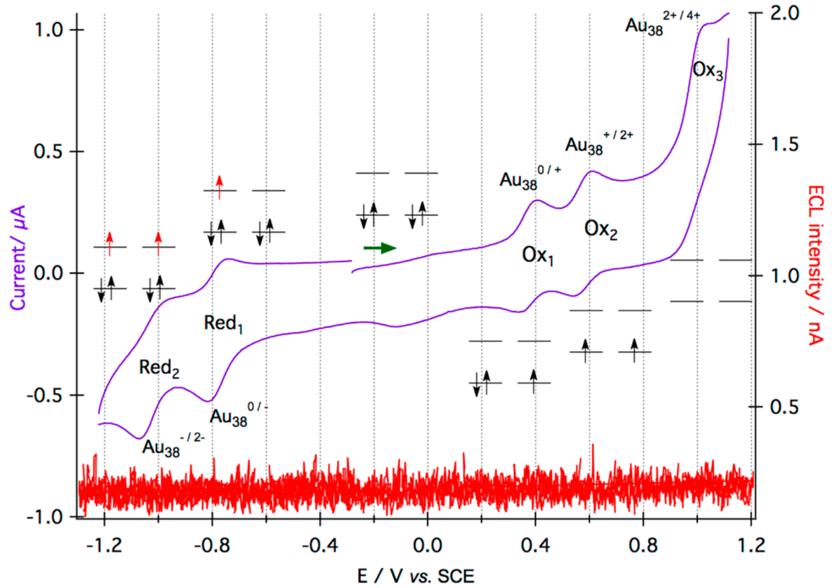

Figure 1. Cyclic voltammogram (purple) and ECL−potential curve (red) of 0.1 mM Au_{38} nanoclusters in 1:1 acetonitrile: benzene mixture containing 0.1 M TBAP, which was recorded in a potential window between −1.28 and 1.22 V *vs* SCE at a scan rate of 100 mVs^{-1}. The arrow indicates the direction of the potential scanning from the start. The insets illustrate the electronic configurations of various redox states where the degeneracy of the HOMOs and LUMOs might be lifted.

with the clusters' HOMO−LUMO energy gaps. Furthermore, we employed spooling ECL spectroscopy to gain insight into the mechanism of the ECL process. In the spooling technique, consecutive ECL spectra are recorded in the course of the applied potential scanning. Any changes in the emission peak wavelength can be tracked to correlate to the corresponding potentials. The observed NIR emission for $Au_{25}(SR)_{18}^{+}$ not only opens up opportunities for it to be utilized in bioanlaytical applications (because the NIR wavelength has low energy and is not absorbed by the live cells and tissues in biological imaging), but also sets the stage to extend the mechanistic study to other charged $Au_{25}(SR)_{18}^{z}$ ($z = -1, 0$) nanoclusters and various sized Au nanoclusters. These studies will provide insight into the effects of the Au cluster core size, its charges and the protecting ligands on the ECL wavelength, intensity and efficiency.

Herein, we report ECL of the very interesting $Au_{38}(SC_2H_4Ph)_{24}^{0}$ (Au_{38}, SC_2H_4Ph = 2-phenylethanethiol) nanocluster, in which the face-fused biicosahedral Au_{23} core differentiates from other studied clusters in that two Au_{13} icosahedra fused together *via* sharing a common Au_3 face.[26] The atomic structure of this nanocluster predicts a HOMO−LUMO gap of 0.9 eV,[8,9] and it exhibits an extremely well-defined electrochemical behavior. These will allow a thorough interrogation of the ECL mechanism in the presence of coreactants. It was discovered that coreactants such as tri-*n*-propylamine (TPrA) and benzoyl peroxide (BPO) enhanced greatly the ECL emission of Au_{38} clusters, while that in the annihilation route was very weak. In the two coreactant reactant systems, either the electrogenerated $TPrA^{\bullet}$ with a high reducing power of ($E° = -1.7$ eV)[27] or the benzoate radical ($C_6H_5CO_2^{\bullet}$) with a high oxidizing power ($E° = +1.5$ eV)[28] reacts with the various defined redox sates of the Au_{38} generated in the anodic (for TPrA) or cathodic (for BPO) potential ranges, respectively. The resulting ECL spectra revealed a peak wavelength at *ca.* 930 nm in the presence of either TPrA or BPO as coreactants. The combination of ECL−potential curves with spooling ECL spectra explicitly elucidated ECL mechanisms, where Au_{38}^{+*}, Au_{38}^{2+*}/ Au_{38}^{3+*} and Au_{38}^{-*} were the electrogenerated excited species emitting light. In the Au_{38}/TPrA coreactant system, the $TPrA^{\bullet}$ reacted with Au_{38}^{2+} and Au_{38}^{3+}/ Au_{38}^{4+} electrogenerated in the anodic region, producing Au_{38}^{+*} and Au_{38}^{2+*}/ Au_{38}^{3+*}. In the cathodic region, the benzoate radical and Au_{38}^{2-} were formed in the Au_{38}/BPO system to produce Au_{38}^{-*}. All these three excited species emitted at the same peak wavelength. This was verified through a careful *in situ* spectrophotoelectrochemical study of these $Au_{38}(SR)_{24}^{z}$ species (z = 2−, 1−, 0, 1+, 2+ and 3+/4+) generated independently *via* electrolysis, at various applied potentials. The above observation and the similarities of the emission for each of the corresponding excited states allow control of the ECL intensity in the NIR region.

RESULTS AND DISCUSSION

Correlating Electrochemistry of the Au_{38} to Its Electronic Configuration. Figure 1 shows the cyclic voltammogram of 0.1 mM Au_{38} in 1:1 acetonitrile:benzene mixture containing 0.1 M tetra-*n*-butylammonium perchlorate (TBAP) as the supporting electrolyte. The Au_{38} undergoes five successive redox reactions in both anodic and cathodic regions with formal potentials of −0.762, −1.010, 0.390, 0.598, and 0.994 V *vs* SCE, assigned as Red_1 (Au_{38}^{0}/Au_{38}^{-}) and Red_2 (Au_{38}^{-}/Au_{38}^{2-}), Ox_1 (Au_{38}^{+}/Au_{38}^{0}), Ox_2 (Au_{38}^{2+}/Au_{38}^{+}), and Ox_3 ($Au_{38}^{3+/4+}/Au_{38}^{2+}$), respectively. The above redox reaction pattern agrees well with that reported by Quinn and Liljeroth *et al.* for their pure Au_{38} prepared using a different method.[8]

Aiken, Häkinnen, Tsukuda and co-workers used experimental powder XRD data and employed DFT calculations[29] to predict along with the Zeng group[30] the structure of the Au_{38} as $Au_{23}@(Au(SR)_2)_3(Au_2(SR)_3)_6$ having a nanorod-like biicosahedral core plus three monomeric staples (RS-Au-SR) and six dimeric staples (RS-Au-S(R)-Au-SR). This prediction was later verified by the Jin group, who successfully isolated and refined the Au_{38} single crystal structure.[26] The calculations of the Au_{38} electronic structure[29] revealed that the Au_{38} has two degenerated HOMOs occupied with four electrons, and two degenerated LUMOs. This information provided the basis of the assignments for the electrochemical features shown in Figure 1.

In the anodic scan, the Au_{38} undergoes two successive reversible one-electron oxidation reactions, as illustrated by the insets for HOMO−LUMO configuration illustrations in Figure 1. Assuming the original energies of the two degenerated HOMOs are maintained upon oxidation, the difference between the formal potentials of the Ox_1 and Ox_2 (0.208 V) is likely the result of less static repulsion and in turn greater driving force needed to remove the second electron after the first oxidation. The Au_{38}^{2+} was further oxidized (Ox_3) irreversibly when the applied potential moved to more positive potentials. From the ratio of the Ox_3 peak current to that of Ox_2, it appears that the next two electrons in the degenerate HOMOs are removed at the same or very similar potential and appear as a single two electron wave (Ox_3 reaction). When the scan rate was increased to 1000 mV/s, it is evident that the first two of the oxidation reactions are reversible; see Figure S3 in the Supporting Information (SI). To further test the reversibility of the Ox_1 and Ox_2 oxidation reactions, CVs for the same Au_{38} solution at various scan rates between 100 and 1000 mV/s were recorded, Figure S4 (SI) (A), where the two oxidation (Ox_1 and Ox_2) waves in a potential window between −0.28 and 0.72 V *vs* SCE, were covered. The anodic and cathodic peak currents were identical for the first two oxidation reactions.

In the cathodic scan, electrons were injected consecutively into the two degenerated LUMOs revealing the Red_1 and Red_2 waves, Figure 1. Similar electrochemical evaluation was performed for Red_1 and Red_2 reactions as above in the potential range of −0.28 to −1.22 V *vs* SCE (Figure S5 (SI)). Red_1 is quasi-reversible (becomes reversible at higher scan rates), which agrees with the results obtained by scanning electrochemical microscopy (SECM),[8] where a EC mechanism for Red_1 with a chemical reaction (desorption of Au-thiol motifs) rate constant for the homogeneous step of 8 s^{-1}. In reference to Red_2, the ligand removal reaction following the electrochemical reduction[13] is faster, however the reduction wave is still quasi-reversible at all scan rates probed.

The HOMO−LUMO gap[29] was determined to be 0.952 eV. This was calculated from the potential difference between the first oxidation and first reduction waves ($E°_{Ox1} - E°_{Red1}$ = 1.158 eV) with an associated charge correction[4] (Ox_1 and Ox_2 potential differences, *ca*. 0.206 eV). This value is close to that determined from the optical HOMO−LUMO gap (0.9 eV) following the method reported previously (see Figure S1 (SI)).[9] Figure S1 (SI) displays the HOMO−1 to LUMO, HOMO−2 to LUMO, and HOMO−2 to LUMO+1 transitions as well, which correlate well to those from theoretical calculations.[30]

ECL in Annihilation Route. Figure 1 also displays the recorded ECL intensity *versus* the applied potential (ECL−potential curve) for the same 0.1 mM Au_{38} cluster electrolyte solution utilized during the potential scanning between −1.22 and 1.13 V *vs* SCE. While the Au_{38} has several accessible redox species with energies that in principle could react to produce ECL, no measurable ECL intensity was detected at varying potentials in this range. This is most likely due to the short lifetime and/or low reactivity of all charged Au_{38} species, electrogenerated during the time scale of this electrochemical scan. Consequently, it is natural to use a coreactant[20] system that can produce strong electrogenerated oxidizing or reducing radicals that are formed at the potentials near to those of the electrogenerated Au_{38} species permitting ET reactions and promoting ECL enhancement. Tri-*n*-propylamine (TPrA)[27,31,32] and benzoyl peroxide (BPO)[28] were selected as coreactant candidates giving the well-known oxidizing and reducing powers of their electrogenerated radical intermediates (*vide supra*).

ECL of the Au_{38} in the Presence of TPrA. Figure 2 displays ECL−potential curve of the above 0.1 mM Au_{38} in the 1:1 acetonitrile:benzene electrolyte solution with 6.3 mM TPrA at a scan rate of 100 mV/s. The ECL onset was at 0.810 V *vs* SCE, at which the Au_{38} was already oxidized to Au_{38}^{2+} ($E^{\circ\prime}$ = 0.598 V *vs* SCE). At this potential, TPrA began to undergo an oxidation reaction[33] (eq 1) producing TPrA radical cation ($TPrA^{\bullet+}$), which then rapidly deprotonated to form TPrA radical ($TPrA^{\bullet}$) (eq 2).[27] The high reducing $TPrA^{\bullet}$, with a reduction power of −1.7 eV as determined by Lai and Bard,[27] injected an electron to the Au_{38}^{2+} LUMO orbital, producing the excited state, Au_{38}^{+*} (eq 3 and the blue inset of Figure 2), that emitted light upon relaxing to the ground state (eq 4). The ECL mechanism is very similar to that in the $Ru(bpy)_3^{2+}$/TPrA coreactant system.[34] Furthermore, ECL in the range of 0.900 and 1.200 V under the brown current segment in Figure 2 is attributed to $Au_{38}^{3+*}/Au_{38}^{2+*}$ (most probably to Au_{38}^{3+*}, due to the indistinguishable two-electron reaction),

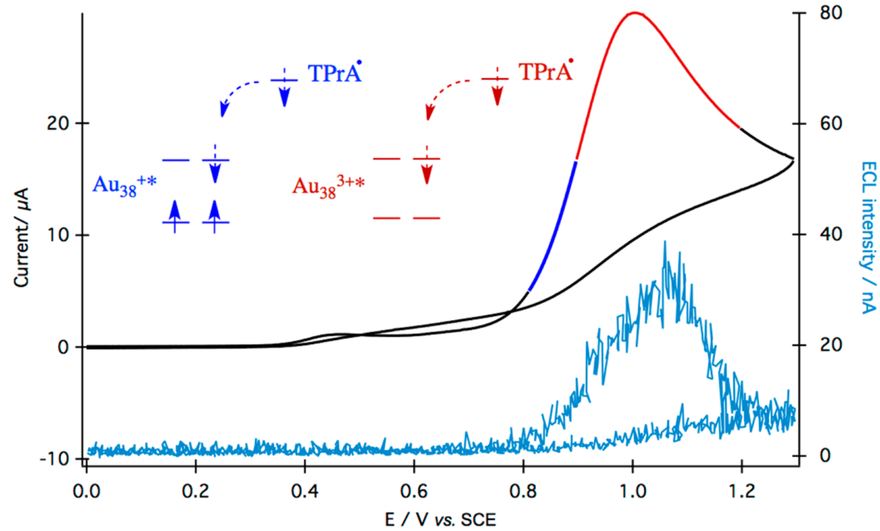

Figure 2. ECL−potential curve of the 0.1 mM Au_{38} nanocluster in 1:1 acetonitrile:benzene mixture containing 0.1 M TBAP in the presence of 6.3 mM tri-*n*-propyl amine (TPrA). The insets show schematic electronic reaction diagrams of Au_{38}^{2+} and $TPrA^{\bullet}$ (blue) as well as Au_{38}^{4+} and $TPrA^{\bullet}$ (brown) to generate excited species Au_{38}^{+*} and Au_{38}^{3+*}, respectively.

eqs 5−8, and the brown inset in Figure 2. The ECL intensity evolution and devolution followed those of $TPrA^{\bullet}$, as illustrated by the color-coded current segments in Figure 2.

$$TPrA \rightarrow TPrA^{\bullet+} + e \quad (1)$$

$$TPrA^{\bullet+} \rightarrow TPrA^{\bullet} + H^{+} \quad (2)$$

$$Au_{38}^{2+} + TPrA^{\bullet} \rightarrow Au_{38}^{+*} + Pr_2N^{+} = CHCH_2CH_3 \quad (3)$$

$$Au_{38}^{+*} \rightarrow Au_{38}^{+} + hv \quad (4)$$

$$Au_{38}^{3+} + TPrA^{\bullet} \rightarrow Au_{38}^{2+*} + Pr_2N^{+} = CHCH_2CH_3 \quad (5)$$

$$Au_{38}^{2+*} \rightarrow Au_{38}^{2+} + hv \quad (6)$$

$$Au_{38}^{4+} + TPrA^{\bullet} \rightarrow Au_{38}^{3+*} + Pr_2N^{+} = CHCH_2CH_3 \quad (7)$$

$$Au_{38}^{3+*} \rightarrow Au_{38}^{2+} + hv \quad (8)$$

The accumulated ECL spectrum (total ECL emission measured during the course of the potential scanning) revealed a very similar peak wavelength (930 nm, 1.33 eV) as that (914 nm, 1.36 eV) of the PL spectrum of a 0.05 mM Au_{38} clusters measured at room temperature (Figure 3). This apparent PL peak wavelength and its shape (*vide infra*) are due to the temperature-induced line broadening as described by Liljeroth, Quinn and co-workers.[35] They elegantly showed that further luminescence peaks can be resolved at very low temperatures, with a peak at 0.98 eV (1266 nm) related to HOMO−LUMO transition that is resonant with the Au_{38} absorption onset (Figure S1 (SI)). The first PL peak is hidden by others at 1.15 eV (1079 nm), 1.26 eV (985 nm), and 1.46 eV (850 nm) related to transitions from larger energy gaps. The nominal PL maximum at 1.36 eV (914 nm) in Figure 3B, which agrees very well with the literature value 1.35 eV (919 nm),[35] sits between relative strong PL peaks at 1.26 eV (985 nm), and 1.46 eV (850 nm). The Whetten's group believed that the photoluminescence mechanism of different sizes of Au nanocrystals involves only gold core electronic states.[36] Therefore, it is unlikely that the luminescence is arising out of the −S−Au−S−Au−S−

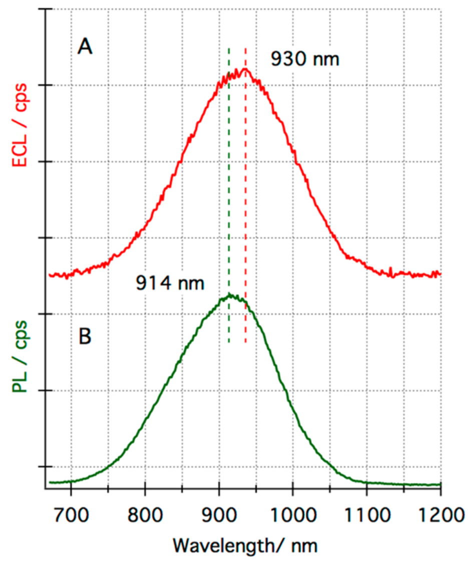

Figure 3. (A) Accumulated ECL spectrum (red) of the 0.1 mM Au_{38} nanocluster electrolyte solution with 6.3 mM TPrA and (B) photoluminescence spectrum (green) of a 0.05 mM Au_{38} in the 1:1 acetonitrile:benzene electrolyte solution. The excitation wavelength for PL was at 532 nm. Both spectra were acquired at room temperature (295 K) using an Andor BR-DD CCD camera cooled at −65 °C and attached to an Acton spectrograph.

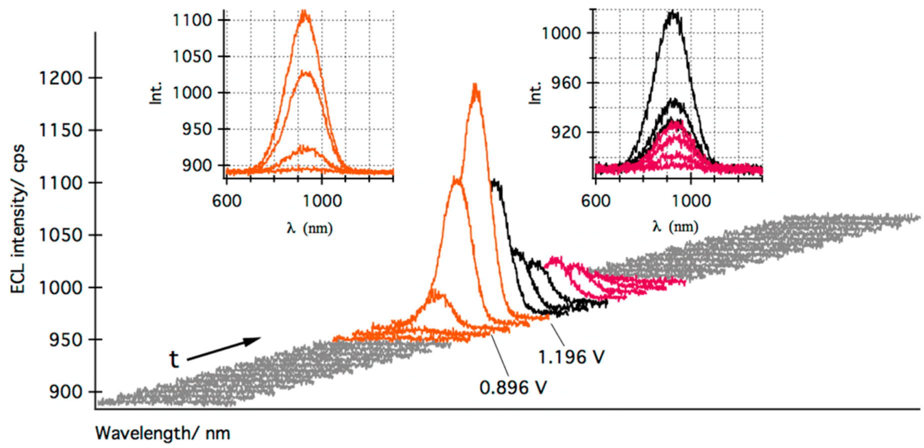

Figure 4. Spooling ECL spectra of 0.1 mM Au_{38} nanoclusters in 1:1 acetonitrile:benzene mixture containing 0.1 M TBAP in the presence of 6.3 mM TPrA at a scan rate of 100 mV/s. The potential window was between −0.51 and 1.3 V *vs* SCE, and each spectrum was recorded in 1 s time interval or 100 mV potential interval. The insets show stacked spectra demonstrating the ECL evolution and devolution in course of the cyclic potential scanning.

or −S−Au−S− staple motifs. However, the Au_{38} excited-state dynamics is complex and might not be a typical two-state relaxation from core to semiring states. It might rather proceed like its counterpart, the Au_{25},[37] through a manifold of electronic states.

The ECL emission observed here might have a similar shape and transmissions to those of the PL process but is masked by the broadening at room temperature, while the 16 nm red shift relative to the PL in Figure 3 is likely due to the self-absorption, as observed in other ECL systems.[20]

To gain further information on the ECL mechanisms of the Au_{38} in the presence of TPrA, we employed spooling ECL spectroscopy that allowed us to track the ECL spectra and intensity as a function of the applied potential (*i.e.*, time) while scanning. Figure 4 presents the spooling ECL spectra of the Au_{38} with 6.3 mM TPrA, in the same potential window as the ECL−potential curve in Figure 2 (−0.51 to 1.3 V *vs* SCE). The insets demonstrate the evolution of the ECL on the anodic scan until 1.196 V (left) and the devolution for the further scanning to 1.300 V and then the return scan (right).

The onset ECL spectrum with a peak wavelength of 930 nm was recorded at 0.896 V, at which potential Au_{38}^{+*} was produced through the reaction illustrated in eq 3. As the applied potential was extended to more positive potentials (*e.g.*, 0.996 V), a resulting higher concentration of $TPrA^{\bullet}$ in the vicinity of the working electrode reacted with electrogenerated Au_{38}^{2+}, leading to an enhanced ECL intensity. It is interesting to note that at higher potentials ($E > 0.996$ V *vs* SCE) at which Au_{38}^{2+} was further oxidized to Au_{38}^{3+} or Au_{38}^{4+}, the ECL intensity increased 5 fold, likely due to the additional involvement of the processes outlined in eqs 5−8. At 1.196 V, the ECL peak intensity reached its maximum (10 times than that at 0.896 V), importantly at the same peak wavelength. In the reverse scan the ECL intensity decreases due to the reverse reactions as well as the resulting depletion of $TPrA^{\bullet}$ and charged Au_{38} species. The trend of ECL evolution and devolution follows that of the ECL−potential curve in Figure 2. Importantly the data suggest that Au_{38}^{+*}, Au_{38}^{2+*}, and Au_{38}^{3+*} likely have the same emission peak wavelength, while the intensities vary due to the different electron populations.

To examine the effect of the relative oxidation states of the Au_{38} on the luminescence intensity and wavelength, we performed an *in situ* spectrophotoelectrochemical study of the 0.1 mM Au_{38}^{0} solution. In this experiment, the applied potential was held at different values corresponding to the various redox states of Au_{38}, illustrated in Figure 1. A 0.1 mM Au_{38} electrolyte solution freshly prepared under Ar atmosphere in a 1 mm thin-layer electrochemical cell. The electrolysis was performed using a Pt mesh as the working electrode, a nonaqueous reference electrode (Ag wire immersed in 0.01 M Ag^{+}/0.1 M TBAP in acetonitrile), and a Pt wire as the counter electrode.[12] The mesh electrode area was excited using a 532 nm laser, and single or spooling photoluminescence spectra were acquired from the narrow side of the thin layer solution by means of the same CCD camera and spectrograph set. This led to the *in situ* formation of the desired charge species $Au_{38}^{3+/4+}$, Au_{38}^{2+}, Au_{38}^{+}, Au_{38}^{-}, and Au_{38}^{2-} at 1.0, 0.65, 0.45, −0.85 and −1.1 V *vs* SCE, respectively (Figure 5B−F). At the same time, spooling PL spectra of the solution were recorded during the electrolysis to help track possible changes in the PL emission wavelength and intensity. Figure 5 shows the PL spectra of the different charge species Au_{38}^{z} (z = 0 (A), 1+ (B), 2+ (C), 3+/4+ (D), 1− (E), and 2− (F)), and the insets illustrate the typical spooling PL spectra accumulated during a continuous potential scanning that is equivalent to an electrolysis. It is evident that there is no significant peak wavelength change as we progress from one charge state to

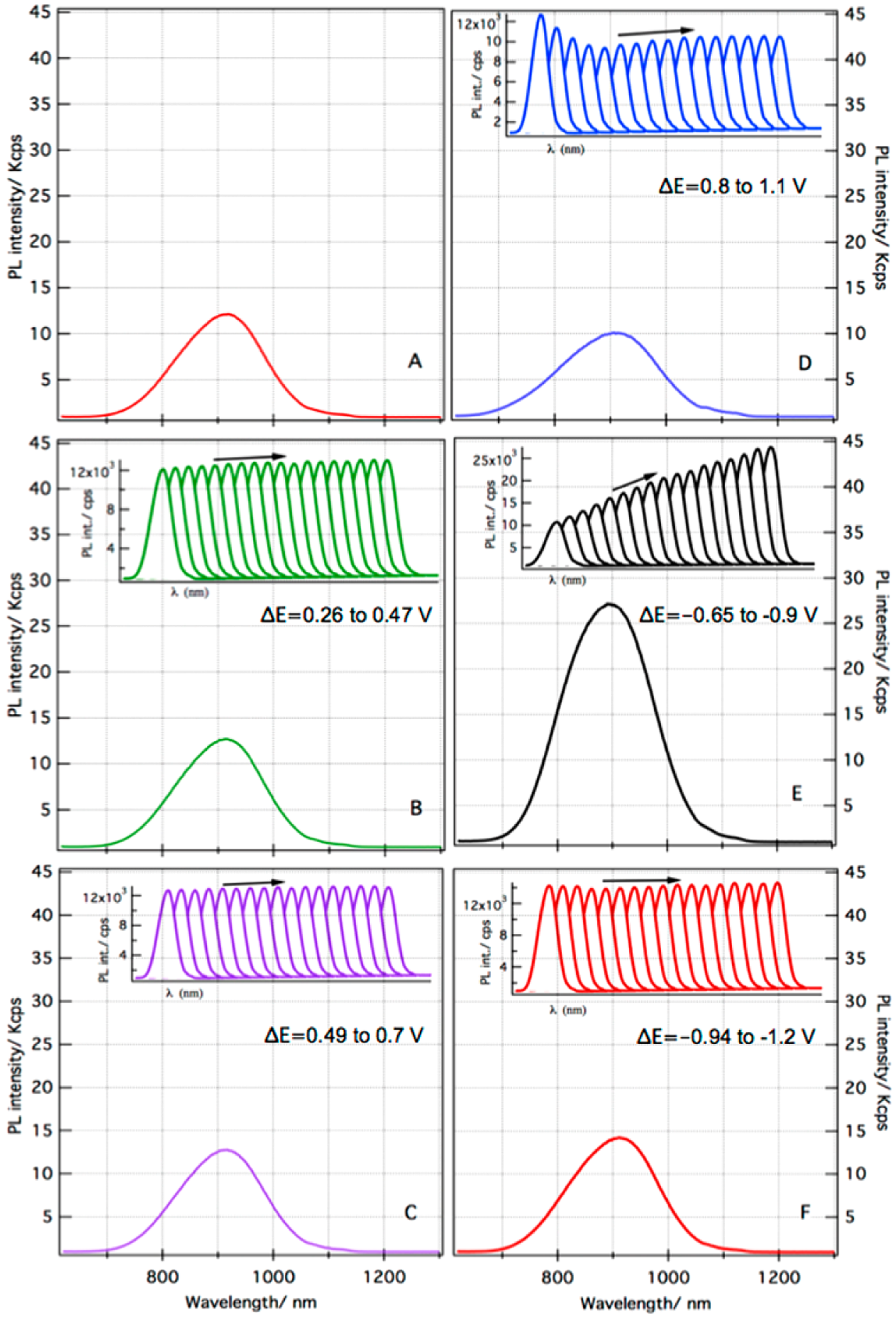

Figure 5. PL spectra of the Au_{38}^{z} (z = 2−, 1−, 0, 1+, 2+, 3+/4+) in 1:1 acetonitrile:benzene mixture containing 0.1 M TBAP using a 1 mm thin layer spectroelectrochemical cell (see Experimental Section). The applied potential was scanned in a range as indicated in each panel, corresponding to Au_{38}^{0}, Au_{38}^{+}, Au_{38}^{2+}, $Au_{38}^{3+/4+}$, Au_{38}^{-}, Au_{38}^{2-}. The insets demonstrate the typical spooling PL spectra in course of a continuous potential scanning at a scan rate of 100 mV/s in a range as indicated by Δ*E*. Each spectrum was acquired for 2 s, and the time interval was 50 s. The arrows indicate the electrolysis time and spooling direction. All samples were excited with a 532 nm laser source.

the next, except that of the Au_{38}^{-} blue-shifted, while the intensity of the PL emission does vary with the charge. Importantly, from Au_{38}^{0} to Au_{38}^{+} and Au_{38}^{2+} there is no notable change in the recorded PL intensity ($PL_{int.}$ ∼ 12 Kcps), while Au_{38}^{3+}/Au_{38}^{4+} shows a decrease to ∼9 Kcps. The Au_{38}^{-} revealed the highest intensity up to 26 Kcps at the end. This could be due to its electronic configuration with one electron in each LUMO, which leads higher probability of transition back to the only HOMO having a vacancy of one

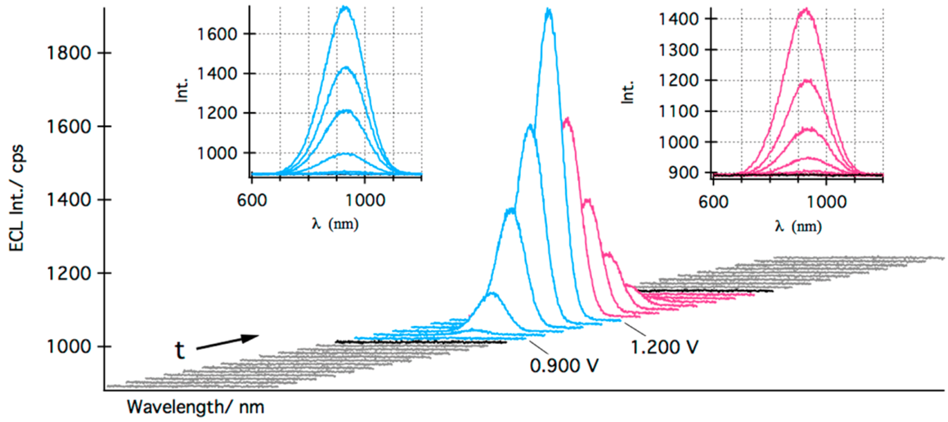

Figure 6. Spooling ECL spectra of the 0.1 mM Au_{38} in 1:1 acetonitrile:benzene mixture containing 0.1 M TBAP with 50 mM TPrA at a scan rate of 100 mV/s. The potential window was between −0.51 and 1.3 V *vs* SCE and each spectrum was recorded in 1 s time interval. The insets show stacked spectra illustrating ECL evolution and devolution during the potential scanning.

electron. Finally, the Au_{38}^{2-} showed basically no change in the course of its formation.

On the basis of above electrochemistry, PL results and assumption that original energies of the two degenerated HOMOs and LUMOs are maintained upon oxidation and reduction, it is plausible that ECL might have the same transitions as those of the PL process and displays the same peak wavelength of 930 nm. Similar to the PL modes of the Au_{25},[37] higher energy core excited states seemed to relax to the semiring states which emitted light upon relaxing to HOMO. The light emission was found to be 930 nm, higher in energy than the HOMO−LUMO gap.

The Au_{38}/TPrA coreactant system was further studied by varying the concentration of TPrA ([TPrA]) from 12.5, to 25, 50, 100, and 200 mM. With the increased [TPrA], the amount of TPrA$^{\bullet}$ was augmented in the vicinity of the electrode at the same potential, thus an increase in ECL intensity was expected. The highest ECL intensity was observed in the presence of 50 mM TPrA, Figure 6. The onset ECL−potential curve was at 0.850 (Figure S6 (SI)) while that in the spooling ECL spectra (Figure 6) was discovered at 0.900 V *vs* SCE. The ECL spectra acquired over the potential scanning remained a constant peak wavelength at 930 nm, indication of similar ECL mechanisms as in the case of Figure 3. The [TPrA] has no appreciable effect on the ECL generation pattern of the coreactant system. Importantly, the ECL peak height with 50 mM TPrA at 1.200 V *vs* SCE is four times higher than that with 6.3 mM TPrA, expected for the generation of a higher concentration of the TPrA radical with increased [TPrA].

The ECL−potential curves along with corresponding spooling ECL spectra of the Au_{38} solution in the presence of 12.5, 25, 100, and 200 mM TPrA are shown in the SI (Figures S7−S10). No appreciable peak wavelength change was observed. In the TPrA concentration range between 6.5 and 50 mM, the higher the TPrA$^{\bullet}$, the faster the reaction rate of the electrogenerated Au_{38} charged species with TPrA$^{\bullet}$ at the same potentials, and thus the higher concentration of the excited sates and the brighter the ECL intensity. The ECL intensity drops if the TPrA concentration is higher than 50 mM, indicating possible quenching of ECL by the TPrA coreactant at very high concentrations; an effect observed in other ECL systems using this coreactant.[27]

The accumulated ECL spectra (A−F) in the presence of TPrA concentrations of 6.2 to 200 mM are shown in Figure 7, which were obtained for two successive cycles of potential scanning between −0.51 to 1.3 V *vs* SCE. It can be noticed that the ECL emissions have the same peak wavelength (930 nm), as confirmed by the spooling experiments. These results are in good agreement with the observed spooling PL spectra obtained after electrolysis (Figure 5).

Figure 8 illustrates a good correspondence between the integrals of ECL−potential curves (black, Figures 2 and S6−S10 (SI)) *vs* time and of the accumulated ECL spectra (red, Figures 3, 6, S7−S10 (SI)) *vs* wavelength in the presence of various [TPrA]. It is worth noting that the highest ECL emission was reached in the presence of 50 mM TPrA, while further increased [TPrA] to 100 and 200 mM decreased ECL intensity, mainly due to the quenching effect caused by the high concentration of the coreactant.[27] The ECL efficiency of the Au_{38}/TPrA system was calculated *versus* $Ru(bpy)_3^{2+}$/TPrA system and shown in Table 1 (see the SI for the methodology). It is exciting to note that a high relative ECL efficiency of >350% was obtained with 50 mM TPrA, disregarding higher values with 100 and 200 mM TPrA. Since the Andor iDUS BR-DD CCD camera has a very similar response sensitivity for both the $Ru(bpy)_3^{2+}$ (emission at 650 nm) and Au_{38} (emission at 930 nm), our ECL efficiency measurements should be very reliable. In contrast, our conventional ECL efficiency determination using a PMT underestimated the values, due to the dramatic depleted PMT sensitivity in the NIR region (see SI for details) with wavelength longer than 830 nm.

Also investigated was the effect of scan rate on ECL of the Au_{38} nanoclusters in the presence of 50 mM TPrA

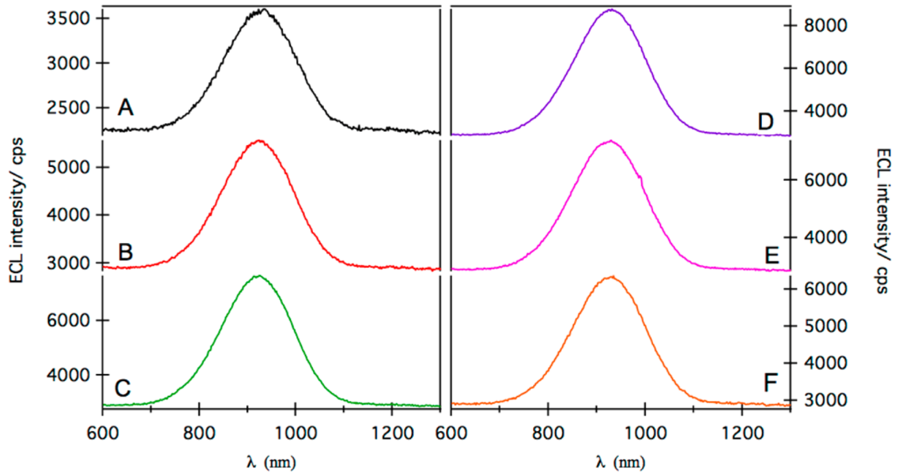

Figure 7. Accumulated ECL spectra for various [TPrA] from 6.3 (A) to 12.5 (B), 25 (C), 50 (D), 100 (E) and 200 (F) mM.

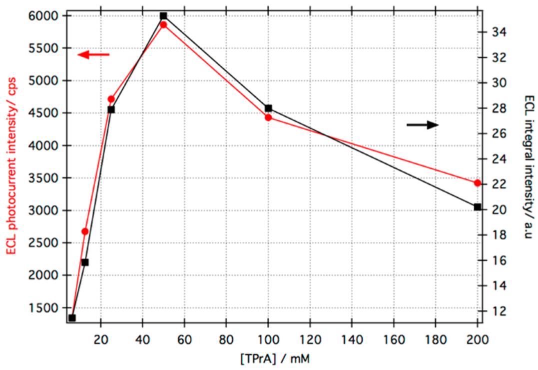

Figure 8. Integrals of ECL−potential curves (acquired using the PMT) *vs* time (black) and ECL intensity (measured by the CCD camera and spectrograph set) *vs* wavelength (red) in the presence of various [TPrA]. These integrated values are equivalent to the numbers of photons emitted.

at 25, 50, 75, 100, 200, and 400 mVs^{-1}, respectively. Figure S11 (SI) shows accumulated ECL spectra and ECL−potential curves along with CVs at the above scan rates. The corresponding ECL spooling spectra (with a time interval of 1 s) are displayed in Figure S12 (SI). The trend illustrates that lower scan rate generates relatively higher ECL intensity in the system. The slower the scan rate, the more the charge injected and the higher the concentrations of the two species that participate the electron transfer reaction (such as eqs 3, 7 and 12) to generate the excited state. The ECL process is photon generation per charge injection and its intensity in general depends on the availability of these species. In addition, the ECL generation depends also on the stability and reactivity of the participating species. From the results in Figures S11 and S12 (SI), it is plausible that the concentration factor dominates in the coreactant system.

ECL of the Au_{38}/BPO Coreactant System. On the basis of the two consecutive electrochemical reduction reactions of the Au_{38} in the cathodic region, it is also of interest to investigate ECL emission in the presence of BPO, from which a strong oxidizing intermediate, benzoate radical ($C_6H_5CO_2^{\bullet}$) with a reduction potential

TABLE 1. Calculated ECL Efficiency for the Au_{38}/TPrA System with Various [TPrA] in Reference to That of $Ru(bpy)_3^{2+}$/TPrA in 1:1 Acetonitrile:Benzene Electrolyte Solution[a]

[TPrA]/mM	ECL eff./%
6.3	13
12.5	24
25	46
50	354
100	591
200	836

[a] Absolute quantum ECL efficiency of $Ru(bpy)_3^{2+}$ is 0.05.

of 1.5 V (eq 9), can be produced.[28] In addition, we have recently reported the ECL of the $Au_{25}(SR)_{18}$ cluster/BPO system.[25] Among various organic soluble coreactant in ECL studies, BPO have been used extensively mainly due to its solubility in majority of organic solvents.

$$BPO + e \rightarrow C_6H_5CO_2^{\bullet} + C_6H_5CO_2^{-} \quad (9)$$

Figure 9A illustrates cyclic voltammogram and ECL−potential curve of 0.1 mM Au_{38} clusters in the presence of 5 mM BPO in 1:1 acetonitrile:benzene mixture. The CV shows a reduction peak at ∼ −1.5 V *vs* SCE, at which $C_6H_5CO_2^{\bullet}$ was generated in the vicinity of the working electrode (eq 9). The ECL onset was at −1.0 V *vs* SCE, indicating electronic interaction between negatively charged species of the $Au_{38,}$ and $C_6H_5CO_2^{\bullet}$. By comparing the reduction potentials of $Au_{38}^{0/-}$ (eq 10) and $Au_{38}^{-/2-}$ (eq 11) with the onset potential value, it can be noticed that at −1.0 V, the $C_6H_5CO_2^{\bullet}$ reacted with Au_{38}^{2-} (eq 12). In fact, the $C_6H_5CO_2^{\bullet}$ accepts an electron from one of the two Au_{38}^{2-} HOMO orbital (the inset in Figure 1), producing the Au_{38}^{-*} excited state. The Au_{38}^{-*} then relaxed to the ground state, emitting light (eq 13). The acquired ECL spectrum displayed a peak wavelength of 930 nm (Figure 9B), very close to what we observed for the Au_{38}/TPrA system. The ECL peak maximum in the ECL−potential curve was found to be at −1.345 V *vs*

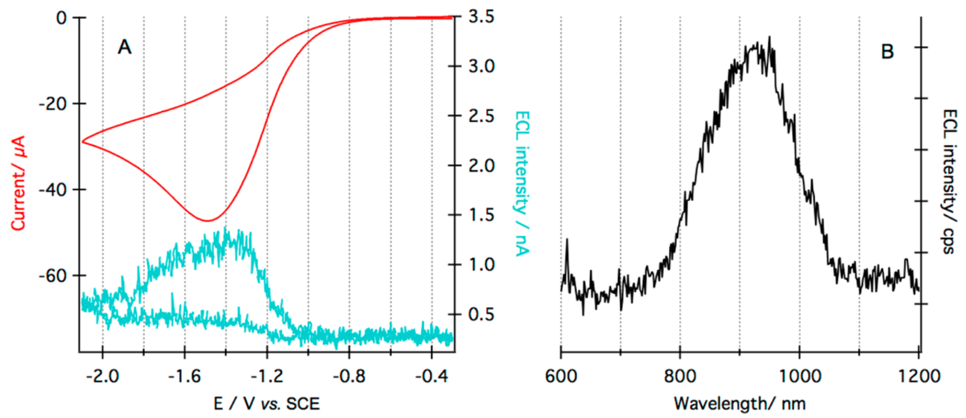

Figure 9. (A) Cyclic voltammogram (red) and ECL−potential curve (teal) of the 0.1 mM Au_{38} electrolyte solution in the presence of 5 mM benzoyl peroxide (BPO). (B) The accumulated ECL spectrum of the same solution recorded on an Andor BR-DD CCD camera cooled at −65 °C and attached to an Acton spectrograph.

SCE, at which the Au_{38} cluster was reduced all the way to Au_{38}^{2-} and the $C_6H_5CO_2^{\bullet}$ reached its maximum concentration in the vicinity of the working electrode. Thus, electron removal from Au_{38}^{2-} HOMOs formed Au_{38}^{-*} (eq 12). The ECL enhancement is related to the high concentrations of both electrogenerated $C_6H_5CO_2^{\bullet}$ and Au_{38}^{2-}. Additionally, the close potential of the reduction of Au_{38} and BPO might lead an efficient interaction between these two species. Therefore, the electrogenerated Au_{38}^{2-} will mostly react with benzoate radical and participate in ECL process, rather than simply involve an EC reaction and lose a ligand (please see the electrochemistry section).

$$Au_{38}^{0} + e \rightarrow Au_{38}^{-} \quad (10)$$

$$Au_{38}^{-} + e \rightarrow Au_{38}^{2-} \quad (11)$$

$$Au_{38}^{2-} + C_6H_5CO_2^{\bullet} \rightarrow Au_{38}^{-*} + C_6H_5CO_2^{-} \quad (12)$$

$$Au_{38}^{-*} \rightarrow Au_{38}^{-} + h\nu \quad (13)$$

The ECL peak wavelength is again in good agreement with that of PL spectrum shown in Figure 6E. This similarity in the peak wavelength suggests that the related ECL and PL relaxation processes and emission through similar mechanisms. The formed Au_{38}^{-} might participate in a catalytic reaction and get reduced again on the electrode surface. The reduction waves of Au_{38}^{-} to Au_{38}^{2-} are less negative than that for $C_6H_5CO_2^{\bullet}$ radical formation. One can argue that this is the main reason for the lower ECL light emission intensity of the Au_{38}/BPO system, while close potentials for the formation of TPrA radical and Au_{38}^{2+} and $Au_{38}^{3+/4+}$, result in higher ECL intensity. The ECL efficiency relative to the $Ru(bpy)_3^{2+}$/BPO system was determined to be 7.2%, which was much lower than that of the $Ru(bpy)_3^{2+}$/TPrA system. Higher concentrations of BPO were also tested. No ECL emission was observed, due to the quenching of ECL by high BPO concentration.[38]

CONCLUSIONS

For the first time the ECL of the Au_{38} cluster is reported, displaying a unique peak wavelength at 930 nm in the NIR region. The results suggest all accessible excited states of Au_{38} cluster emit at the same wavelength, which was unambiguously corroborated from the *in situ* spectrophotoelectrochemistry. It was also revealed that among the charged Au_{38} species, the Au_{38}^{-} generates the highest PL intensity. The short lifetime of both the electrogenerated Au_{38}^{2-} and $Au_{38}^{3+/4+}$ species or their reactivity limited ECL emission in the annihilation route. Coreactants such as TPrA and BPO greatly enhanced the ECL emissions. Spooling ECL spectroscopy confirmed that and Au_{38}^{+*} (and Au_{38}^{3+*}) and Au_{38}^{-*} were involved in the ECL emission processes in the presence of TPrA and BPO, respectively. Also, the accumulated ECL spectra showed that ECL emission peak wavelengths, at ∼930 nm in NIR region, does not change by altering the TPrA concentration or the applied potential. Interestingly, the ECL intensity can be tuned by changing the coreactant concentration or working electrode potential. ECL efficiency was determined to be 3.5 times higher than that of the $Ru(bpy)_3^{2+}$/TPrA system. It is anticipated that the NIR-ECL of the Au_{38} clusters will find electroanalytical applications in imaging of live cells.

EXPERIMENTAL SECTION

Chemicals. Hydrogen tetrachloroaurate trihydrate (Aldrich, 99.9%), phenylethanethiol (Aldrich, 98%), sodium borohydride (Aldrich, 99%), methanol (Caledon, 99.8%), trans-2-[3-(4-*tert*-butylphenyl)-2-methyl-2-propenylidene]-malononitrile (DCTB, Aldrich 98%), ethanol (Caledon, 99.8%), and acetonitrile (Caledon) were used as received. Tetra-*n*-butylammonium perchlorate was provided by Fluka (99%) and kept in dedicator before use. Anhydrous acetonitrile (99.8%) and anhydrous benzene (99.8%), benzoyl peroxide (Luperox A98, 98%), Tri-*n*-propylamine (Aldrich, 98%) were purchased from Aldrich.

Synthesis of $Au_{38}(SC_2H_4Ph)_{24}$ Clusters. Monodispersed Au_{38} clusters were prepared according to size selecting synthetic procedure with some modification.[9] Briefly, 196.6 mg (0.5 mmol) $HAuCl_4 \cdot 3H_2O$ and 614.0 mg (2.0 mmol) glutathione powder were mixed in 20 mL of acetone at room temperature, which was stirred for 20 min. The resulted yellowish cloudy suspension was then cooled to 0 °C and kept for another 20 min. A solution of $NaBH_4$ (5 mmol, 189.0 mg, dissolved in 6 mL of cold deionized water) was rapidly added to the suspension under vigorous stirring. The color of the solution immediately turned black after the addition, indicating the formation of clusters. The black $Au_n(SG)_m$ intermediate clusters were found to precipitate out and stick to the inner wall of the flask. The supernatant was then decanted and the residual was dried. The obtained $Au_n(SG)_m$ was redispersed in 6 mL of nanopure water, to which a mixture of 0.6 mL of ethanol, 2 mL of toluene, and 2.5 mL of phenylethenethiol was added. The biphasic solution was heated to and maintained at 80 °C under reflux for overnight. It has been observed that by following the previously reported procedure by Qian's protocol a metallic layer of gold is formed on the reaction flask after 40 h reflux. This is an indication of decomposition of the desired product, when the protecting ligand removes from the gold clusters under the thermal condition. Thus, we increased phenyethene thiol ratio slightly higher (2.5 mL) with a shorter reaction time (18 h at 80 °C) to prevent the desired product decomposition. Our modification led to the formation of desired Au_{38} clusters overnight with ~30% yield based on elemental Au. The UV−vis spectrum of the crude product was measured after 18 h and compared to the reported spectrum.[9] Then, the reaction was cooled down and the mixture was extracted for several times with toluene, and the organic phase was extracted using dichloromethane and collected. The toluene was evaporated under a vacuum, and a dark green crude oily product formed. The solid was obtained after washing the oily crude product thoroughly with methanol to remove excess of the thiol. The pure $Au_{38}(SC_2H_4Ph)_{24}$ clusters were extracted using dichloromethane and characterized by UV−vis−NIR spectroscopy and Matrix assisted laser desorption/ionization mass spectrometry. The UV−vis−NIR spectrum of the pure compound showing distinct features of Au_{38} clusters with peak wavelength at 478 (2.60 eV), 626 (1.98 eV), 743 (1.66) and 1028 (1.20 eV) nm (Figure S1 (SI)). The MALDI spectrum showed a parent peak at 10776.0 Da (Cal. 10778.0 Da) and other peaks produced after removal of $Au_4(SR)_4$ fragments (Figure S2 (SI)).

Characterization. UV−vis−NIR spectra were recorded using a Varian Cary 5000 spectrophotometer. An AB Applied Biosystem mass spectrometer (4700 Proteomics Analyzer) was employed to obtain the MALDI-TOF spectra. The sample was prepared by mixing 0.2:1000 analyte to matrix ratio. Then, 7 μL of the mixture was casted on the target plate and air-dried.

Electrochemistry and ECL Instrumentations. The electrochemistry and ECL of the $Au_{38}(SC_2H_4Ph)_{24}$ cluster were carried out using a 2 mm diameter Pt disc inlaid in a glass sheath as the working electrode (WE), a coiled Pt wire as the counter electrode (CE), and a coiled Pt wire as the quasi-reference electrode (QRE). After each experiment, the electrochemical potential window was calibrated using ferrocence as the internal standard. The redox potential of the ferrocene/ferrocenium (Fc/Fc^+) couple was taken as 0.424 V *vs* SCE.[39] In annihilation ECL studies, a solution containing approximately 3 mg of Au_{38} clusters, 0.1 M TBAP as the supporting electrolyte and 1.5 mL anhydrous acetonitrile and anhydrous benzene was added to the electrochemical cell with a flat Pyrex window at the bottom for detection of generated ECL, which was assembled in a glovebox. For coreactant studies, 5.0×10^{-3} M BPO was added to the annihilation solution and the air-tighten cell was also assembled in a drybox. Different concentrations of TPrA were also added to the electrochemical cell under Ar (99.999%) blanket to prevent oxygen entering the sample solution.

The cyclic voltammetry was performed on a CHI 610A electrochemical analyzer (CH Instruments, Austin, TX). The general experimental parameters for cyclic voltammograms (CVs) are listed here as follows: 0.000 V initial potential in experimental scale, positive or negative initial scan polarity, 0.1 V s^{-1} scan rate, 4 sweep segments, 0.001 V sample interval, 2 s quiet time, 1.5×10^{-5} AV^{-1} sensitivity. The ECL−potential curves were obtained using the CHI 610A coupled with a photomultiplier tube (PMT, R928, Hamamatsu, Japan) held at −750 V with a high voltage power supply. The ECL was collected by the PMT under the flat Pyrex window at the bottom of the cell was measured as a photocurrent, and transformed to a voltage signal, using a picoammeter/voltage source (Keithley 6487, Cleveland, OH). The potential, current signals from the electrochemical workstation, and the photocurrent signal from the picoammeter were sent simultaneously through a DAQ board (DAQ 6052E, National Instruments, Austin, TX) to a computer. The data acquisition system was controlled from a custom-made LabVIEW program (ECL_PMT610a.vi, National Instruments, Austin, TX). The photosensitivity on the picoammeter was set manually in order to avoid the saturation.

The ECL spectra were recorded using the Andor Technology program. Similar to the CV experiments, the samples were scanned between their redox potentials. Since the ECL is in NIR region, ECL spectroscopy was conducted on an Acton 2300i spectrograph with two gratings (50 *l*/mm blazed at 600 nm and 300 *l*/mm blazed at 700 nm) and an Andor iDUS CCD camera (Model DU401-BR-DD-352). The set of the spectrograph and camera was calibrated using a mercury lamp each time. The accumulation spectra were recorded during two successive potential scan cycles as discussed in each experiment. The spooling ECL spectra were acquired at a time interval of 1 s or a potential increment of 100 mV with the potential scan rate of 100 mVs^{-1}.

***In Situ* Spectrophotoelectrochemistry.** The photoluminescence spectra of various Au_{38} charge states (Figure 5) were obtained in the course of electrolysis using 1 mm thin layer quartz cell (BASi) containing the same 0.1 mM Au_{38} electrolyte solution used in the electrochemical and ECL studies, freshly prepared under Ar atmosphere. The electrolysis was performed using a Pt mesh as the working electrode, a nonaqueous reference electrode (Ag wire immersed in 0.01 M Ag^+/0.1 M TBAP in acetonitrile), and a Pt wire as the counter electrodes.[12] The mesh electrode area was excited using a 532 nm laser, and single or spooling photoluminescence spectra were acquired from the narrow side of the thin layer solution by means of the same CCD camera and Acton spectrograph set. A long-pass edge filter was placed between the sample and the spectrograph entrance to cut the excitation wavelength and harmonic peaks.

Conflict of Interest: The authors declare no competing financial interest.

Acknowledgment. We are very grateful to the Department of Chemistry, the Chemistry Electronic Shop and ChemBio Store at Western for the quality support and services. We also thank NSERC-DG and The University of Western Ontario for the financial support to this research.

Supporting Information Available: UV−vis−NIR and MALDI spectra of $Au_{38}(SC_2H_4Ph)_{24}$, full scale CVs of Au_{38} clusters at 100 and 1000 mV/s, CVs of Au_{38} clusters at different scan rates in anodic and cathodic regions, ECL−potential curve of the Au_{38} with 50 mM TPrA, ECL−potential curve and spooling spectra of the Au_{38} with 25, 100, and 200 mM TPrA, accumulated ECL spectra and ECL−potential curves of Au_{38} in the presence 50 mM TPrA at different scan rates, spooling ECL spectra of Au_{38} in the presence 50 mM TPrA at different scan rates, photoluminescence and accumulated ECL spectrum of Au_{38} with 5 mM BPO, spectrum response curves for the PMT and iDus CCD camera. This material is available free of charge *via* the Internet at http://pubs.acs.org.

REFERENCES AND NOTES

1. Philip, R.; Chantharasupawong, P.; Qian, H.; Jin, R.; Thomas, J. Evolution of Nonlinear Optical Properties: From Gold Atomic Clusters to Plasmonic Nanocrystals. *Nano Lett.* **2012**, *12*, 4661–4667.
2. Zhu, M.; Qian, H.; Meng, X.; Jin, S.; Wu, Z.; Jin, R. Chiral Au_{25} Nanospheres and Nanorods: Synthesis and Insight into the Origin of Chirality. *Nano Lett.* **2011**, *11*, 3963–3969.

3. Devadas, M. S.; Bairu, S.; Qian, H.; Sinn, E.; Jin, R.; Ramakrishna, G. Temperature-Dependent Optical Absorption Properties of Monolayer-Protected Au_{25} and Au_{38} Clusters. *J. Phys. Chem. Lett.* **2011**, *2*, 2752–2758.
4. Lee, D.; Donkers, R. L.; Wang, G.; Harper, A. S.; Murray, R. W. Electrochemistry and Optical Absorbance and Luminescence of Molecule-like Au_{38} Nanoparticles. *J. Am. Chem. Soc.* **2004**, *126*, 6193–6199.
5. Knoppe, S.; Dass, A.; Burgi, T. Strong Non-linear Effects in the Chiroptical Properties of the Ligand-Exchanged Au_{38} and Au_{40} Clusters. *Nanoscale* **2012**, *4*, 4211–4216.
6. Qian, H.; Zhu, M.; Wu, Z.; Jin, R. Quantum Sized Gold Nanoclusters with Atomic Precision. *Acc. Chem. Res.* **2012**, *45*, 1470–1479.
7. Murray, R. W. Nanoelectrochemistry: Metal Nanoparticles, Nanoelectrodes, and Nanopores. *Chem. Rev.* **2008**, *108*, 2688–2720.
8. Toikkanen, O.; Ruiz, V.; Ronnholm, G.; Kalkkinen, N.; Liljeroth, P.; Quinn, B. M. Synthesis and Stability of Monolayer-Protected Au_{38} Clusters. *J. Am. Chem. Soc.* **2008**, *130*, 11049–11055.
9. Qian, H.; Zhu, Y.; Jin, R. Size-Focusing Synthesis, Optical and Electrochemical Properties of Monodisperse $Au_{38}(SC_2H_4Ph)_{24}$ Nanoclusters. *ACS Nano* **2009**, *3*, 3795–3803.
10. Jin, R. The Impacts of Nanotechnology on Catalysis by Precious Metal Nanoparticles. *Nanotechnol. Rev.* **2012**, *1*, 31–56.
11. Antonello, S.; Hesari, M.; Polo, F.; Maran, F. Electron Transfer Catalysis with Monolayer Protected Au_{25} Clusters. *Nanoscale* **2012**, *4*, 5333–5342.
12. Kauffman, D. R.; Alfonso, D.; Matranga, C.; Qian, H.; Jin, R. Experimental and Computational Investigation of Au_{25} Clusters and CO_2: A Unique Interaction and Enhanced Electrocatalytic Activity. *J. Am. Chem. Soc.* **2012**, *134*, 10237–10243.
13. Kauffman, D. R.; Alfonso, D.; Matranga, C.; Li, G.; Jin, R. Photomediated Oxidation of Atomically Precise $Au_{25}(SC_2H_4Ph)_{18}^-$ Nanoclusters. *J. Phys. Chem. Lett.* **2013**, *4*, 195–202.
14. Jin, R. Quantum Sized, Thiolate-Protected Gold Nanoclusters. *Nanoscale* **2010**, *2*, 343–362.
15. Zeng, C.; Liu, C.; Pei, Y.; Jin, R. Thiol Ligand-Induced Transformation of $Au_{38}(SC_2H_4Ph)_{24}$ to $Au_{36}(SPh\text{-}t\text{-}Bu)_{24}$. *ACS Nano* **2013**, *7*, 6138–6145.
16. Zeng, C.; Li, T.; Das, A.; Rosi, N. L.; Jin, R. Chiral Structure of Thiolate-Protected 28-Gold-Atom Nanocluster Determined by X-ray Crystallography. *J. Am. Chem. Soc.* **2013**, *135*, 10011–10013.
17. Jadzinsky, P. D.; Calero, G.; Ackerson, C. J.; Bushnell, D. A.; Kornberg, R. D. Structure of a Thiol Monolayer-Protected Gold Nanoparticle at 1.1 Å Resolution. *Science* **2007**, *318*, 430–433.
18. Crasto, D.; Dass, A. Green Gold: $Au_{30}(S\text{-}t\text{-}C_4H_9)_{18}$ Molecules. *J. Phys. Chem. C* **2013**, *117*, 22094–22097.
19. Bard, A. J.; Faulkner, L. R. *Electrochemical Methods: Fundamental and Applications*, 2nd ed.; John Wiley & Sons: New York, 2001.
20. Bard, A. J. *Electrogenerated Chemiluminescence*; Marcel Dekker: New York, 2004.
21. Sardesai, N. P.; Barron, J. C.; Rusling, J. F. Carbon Nanotube Microwell Array for Sensitive Electrochemiluminescent Detection of Cancer Biomarker Proteins. *Anal. Chem.* **2011**, *83*, 6698–6703.
22. Chikkaveeraiah, B. V.; Bhirde, A. A.; Morgan, N. Y.; Eden, H. S.; Chen, X. Electrochemical Immunosensors for Detection of Cancer Protein Biomarkers. *ACS Nano* **2012**, *6*, 6546–6561.
23. Zamolo, V. A.; Valenti, G.; Venturelli, E.; Chaloin, O.; Marcaccio, M.; Boscolo, S.; Castagnola, V.; Sosa, S.; Berti, F.; Fontanive, G.; *et al.* Highly Sensitive Electrochemiluminescent Nanobiosensor for the Detection of Palytoxin. *ACS Nano* **2012**, *6*, 7989–7997.
24. Miao, W. Electrogenerated Chemiluminescence and Its Biorelated Applications. *Chem. Rev.* **2008**, *108*, 2506–2553.
25. Swanick, K. N.; Hesari, M.; Workentin, M. S.; Ding, Z. Interrogating Near-Infrared Electrogenerated Chemiluminescence of $Au_{25}(SC_2H_4Ph)_{18}^+$ Clusters. *J. Am. Chem. Soc.* **2012**, *134*, 15205–15208.
26. Qian, H.; Eckenhoff, W. T.; Zhu, Y.; Pintauer, T.; Jin, R. Total Structure Determination of Thiolate-Protected Au_{38} Nanoparticles. *J. Am. Chem. Soc.* **2010**, *132*, 8280–8281.
27. Lai, R. Y.; Bard, A. J. Electrogenerated Chemiluminescence. 70. The Application of ECL to Determine Electrode Potentials of Tri-*n*-propylamine, Its Radical Cation, and Intermediate Free Radical in MeCN/Benzene Solutions. *J. Phys. Chem. A* **2003**, *107*, 3335–3340.
28. Chandross, E. A.; Sonntag, F. I. Chemiluminescent Electron-Transfer Reactions of Radical Anions. *J. Am. Chem. Soc.* **1966**, *88*, 1089–1096.
29. Lopez-Acevedo, O.; Tsunoyama, H.; Tsukuda, T.; Häkkinen, H.; Aikens, C. M. Chirality and Electronic Structure of the Thiolate-Protected Au_{38} Nanocluster. *J. Am. Chem. Soc.* **2010**, *132*, 8210–8218.
30. Pei, Y.; Gao, Y.; Zeng, X. C. Structural Prediction of Thiolate-Protected Au_{38}: A Face-Fused Bi-icosahedral Au Core. *J. Am. Chem. Soc.* **2008**, *130*, 7830–7832.
31. Zu, Y.; Bard, A. J. Electrogenerated Chemiluminescence. 66. The Role of Direct Coreactant Oxidation in the Ruthenium Tris(2,2′)bipyridyl/Tripropylamine System and the Effect of Halide Ions on the Emission Intensity. *Anal. Chem.* **2000**, *72*, 3223–3232.
32. Kumar, S. S.; Bard, A. J. Background Emission of Electrogenerated Chemiluminescence during Oxidation of Tri-*n*-propylamine from the Dimeric $^1\Delta_g$ State of O_2. *Anal. Chem.* **2012**, *85*, 292–295.
33. Mann, C. K. Cyclic Stationary Electrode Voltammetry of Some Aliphatic Amines. *Anal. Chem.* **1964**, *36*, 2424–2426.
34. Miao, W.; Choi, J.; Bard, A. Electrogenerated Chemiluminescence 69: The Tris(2,2′-bipyridine)ruthenium(II), (Ru(bpy)(3)-(2+))/Tri-*n*-propylamine (TPrA) System Revisited—A New Route Involving $TPrA^{\bullet+}$ Cation Radicals. *J. Am. Chem. Soc.* **2002**, *124*, 14478–14485.
35. van Wijngaarden, J. T.; Toikkanen, O.; Liljeroth, P.; Quinn, B. M.; Meijerink, A. Temperature-Dependent Emission of Monolayer-Protected Au_{38} Clusters. *J. Phys. Chem. C* **2010**, *114*, 16025–16028.
36. Bigioni, T. P.; Whetten, R. L.; Dag, O. Near-Infrared Luminescence from Small Gold Nanocrystals. *J. Phys. Chem. B* **2000**, *104*, 6983–6986.
37. Devadas, M. S.; Kim, J.; Sinn, E.; Lee, D.; Goodson, T.; Ramakrishna, G. Unique Ultrafast Visible Luminescence in Monolayer-Protected Au_{25} Clusters. *J. Phys. Chem. C* **2010**, *114*, 22417–22423.
38. Choi, J.-P. Electrogenerated Chemiluminescence with Amine and Benzoyl Peroxide Coreactants: Reactivity and Reaction Mechanism Studies. Ph.D. Dissertation, The University of Texas at Austin, Austin, TX, 2003.
39. Sahami, S.; Weaver, M. J. Entropic and Enthalpic Contributions to the Solvent Dependence of the Thermodynamics of Transition-Metal Redox Couples: Part I. Couples Containing Aromatic Ligands. *J. Electroanal. Chem.* **1981**, *122*, 155–170.